Journal of Neuroscience Methods 253 (2015) 233–243

Contents lists available at ScienceDirect

Journal of Neuroscience Methods

journal homepage: www.elsevier.com/locate/jneumeth

Computational Neuroscience

Diagnostic tools for evaluating the impact of Focal Axonal Swellings arising in neurodegenerative diseases and/or traumatic brain injury

Pedro D. Maia[a,*], Matthew A. Hemphill[b], Brendan Zehnder[a], Chenfei Zhang[a], Kevin K. Parker[b], J. Nathan Kutz[a]

[a] Department of Applied Mathematics, University of Washington, Seattle, WA 98195-3925, United States
[b] Disease Biophysics Group, Wyss Institute for Biologically Inspired Engineering, Harvard University, Cambridge, MA 02138, United States

HIGHLIGHTS

- Focal Axonal Swellings (FAS) are pathological features of several brain disorders.
- The shape of the FAS play crucial role in spike train propagation impairments.
- Our MATLAB toolbox highlights potential trouble spots along axon images.
- Promising starting point for novel diagnostic techniques.

ARTICLE INFO

Article history:
Received 24 March 2015
Received in revised form 29 June 2015
Accepted 30 June 2015
Available online 16 July 2015

Keywords:
Focal Axonal Swelling
Traumatic brain injury
Concussions
Parkinson
Alzheimer
Multiple Sclerosis
Spike train propagation

ABSTRACT

Background: Focal Axonal Swellings arise in several leading neurodegenerative diseases of the central nervous system and are hallmark features of concussions and traumatic brain injuries. Recent theories mapped how the shape of each swelling affects the propagation of spike trains and consequently the information encoded in them. Spikes can be selectively deleted, have their speed affected, or blocked depending upon the severity of the swelling.
New method: Our computational toolbox extracts meaningful geometrical parameters from sequential images of injured axon segments. The algorithm provides a principled approach for dealing with imaging distortions caused by experimental artifacts in order to extract the cross-section of an axon by detecting local symmetries, turning points and turning regions.
Results: Our characterization of the Focal Axonal Swelling allows for an assessment of its impact on spike propagation, leading to a color coding of the axon that highlights problematic regions for information propagation.
Comparison with existing methods: Many theoretical works reported distortions in spike propagation related to axonal enlargements. Such estimates, however, were not incorporated to a toolbox that could classify axonal swellings directly from experimental images.
Conclusions: Our MATLAB toolbox thus highlights potential trouble spots of axonal morphology, and similar to car traffic maps, identify blocked or impaired routes for information flow. This computational framework is a promising starting point for diagnosing and assessing the impact of axonal swellings implicated in concussions, Alzheimer's and Parkinson's disease, Multiple Sclerosis and other neurological pathologies.

1. Introduction

The existence of discrete swellings along the axon, termed Focal Axonal Swellings (FAS), is widely documented in multiple pathologies including Alzheimer's (Tsai et al., 2004; Krstic and Knuesel, 2012), Parkinson's (Galvin et al., 1999), Creutzfeldt-Jakob's (Liberski and Budka, 1999), HIV dementia (Adle-Biassette

* Corresponding author. Tel.: +1 206 543 5493.
E-mail addresses: pedro.doria.maia@gmail.com (P.D. Maia), matt.hemphill@gmail.com (M.A. Hemphill), brendan.zehnder@gmail.com (B. Zehnder), kkparker@seas.harvard.edu (K.K. Parker), kutz@uw.edu (J.N. Kutz).

http://dx.doi.org/10.1016/j.jneumeth.2015.06.022
0165-0270/

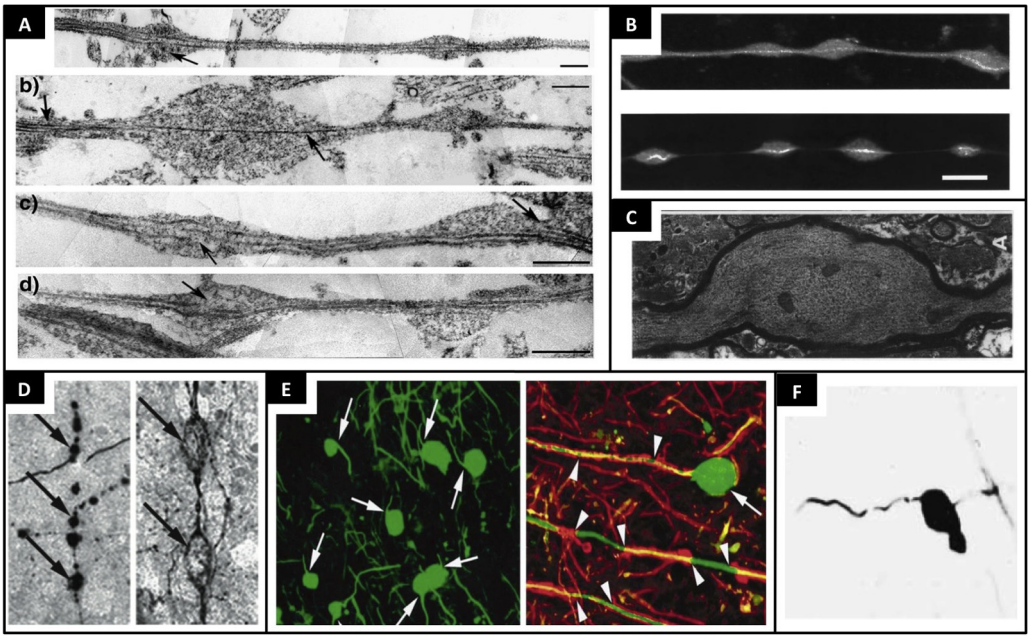

Fig. 1. Focal Axonal Swellings (FAS) arise in several neurodegenerative diseases, concussions and traumatic brain injuries. Panel A: Transmission electron microscopy image of axons 3 h post-stretch injury. Modified from Tang-Schomer et al. (2012). Panel B: Image 2 h after dynamic stretch injury of two human neuron populations. Modified from Smith et al. (1999). Panel C: Image 1 h after stretch injury to guinea pig optic nerve. Modified from Maxwell et al. (1997). The in-vitro stretch injury experiments from Panels A–C mimic the effects of traumatic brain injuries and concussions. Panel D: Axonal swellings are implicated in patients with Alzheimer' s disease where stress-induced amyloidal precursor protein accumulates in axonal compartments. Modified from Krstic and Knuesel (2012). Panels E and F: Images of FAS pathologies in Multiple Sclerosis. Modified from Trapp et al. (1998) and Ferguson et al. (1997).

et al., 1999) and Multiple Sclerosis (Ferguson et al., 1997; Trapp et al., 1998). They are also a hallmark feature of concussions and traumatic brain injury (TBI) – the leading cause of death among youngsters worldwide and a lightning rod issue in contact sports (Fainaru-Wada and Fainaru, 2013). Further, TBI is the signature injury of the wars in Iraq and Afghanistan, affecting a large percentage of returning veterans (Jorge et al., 2012; Xiong et al., 2013). Fig. 1 depicts a number of FAS resulting from TBI and a variety of different neurodegenerative diseases where they are often used as diagnostic markers (Millecamps and Julien, 2013; Coleman, 2005). However, the impact that focal swellings have on both neuronal and neural network function is unknown. Therefore, there is a pressing need to understand how axon morphology relates to its ability to function as a conduit for action potential propagation (Maia and Kutz, 2014a,b; Kolaric et al., 2013).

Many factors can ultimately influence cell morphology, and several have been reported to influence FAS (Johnson et al., 2013; Morrison et al., 2011). TBI studies have demonstrated that FAS can result in up to a 30-fold increase in axon diameter, potentially due to impaired axonal transport at sites of mechanical trauma (Tang-Schomer et al., 2012, 2010). Cellular membrane blebbing has been documented as a precursor to cell death occurring as the cell cytoskeleton degrades (Smith et al., 1999; Maxwell et al., 1997). Many studies report cognitive, behavioral, perceptual and sensory-motor impairments coinciding with the presence of FAS, yet no framework exists to explain the link between these macro-scale behavioral symptoms and the underlying micro-scale pathology (Magdesian et al., 2012; Hemphill et al., 2011).

In this work we quantify the impact of FAS on information encoding at the individual neuron level, creating novel metrics for evaluating cognitive impairments. Recent computational studies show how geometrical properties of FAS can alter their ability to faithfully transmit spike train encodings by selectively deleting spikes, affecting their speed, reflecting spikes at the swelling or even completely blocking spike trains altogether (Maia and Kutz, 2014b,a) (see Section 2.1 for details). We develop a series of algorithms that extract the required geometrical parameters from axonal images and color-code FAS according to how severely they are expected to jeopardize the transmitted information. The effects of injuries in the neuronal network are visualized much like live traffic maps that indicate blocked and/or congested roads.

To demonstrate the method, we applied our MATLAB toolbox to (i) 11 axon segments of uninjured hippocampal rat neurons with rich geometrical structures (see Fig. 2A and Shepherd and Harris, 1998) and (ii) some of our own in vitro injured axons from magnetic twisting cytommetry experiments (Hemphill et al., 2011, 2015). Fig. 2 depicts in detail some of the axons that are used for quantifying the effects of FAS. The figure also shows how the methodology presented can be used as an evaluation tool for quantifying the statistical distribution of swellings, thus providing a neuronal traffic map of signal propagation (or transmitted loss) for individual axons as a function of time. Specifically, areas of compromised information transmission are color coded from yellow to red to black depending upon the level of injury. It also shows that information propagation changes as a function of time as swellings grow. Fig. 2B represents the key diagnostic tool achieved in this work. We expect this simple-to-use toolbox to be of broad interest to the neuroscience, neurological and biomedical engineering communities due to the critical role that Focal Axonal Swellings play in modulating the transmission of information in traumatic brain injuries and/or neurodegenerative diseases.

The paper is outlined as follows. In Section 2, we review the role of axonal geometry in spike-train propagation, from the perspective of formulating a theoretical model to address their spatiotemporal dynamics. Section 3 follows this theoretical framing by considering how geometrical parametrizations of the axons are accomplished in practice. In particular, methods to extract geometrical parameters from real data are of vital importance for evaluating loss of information and eventual cognitive deficits. Section 4 combines the methods of the preceding sections to simulate

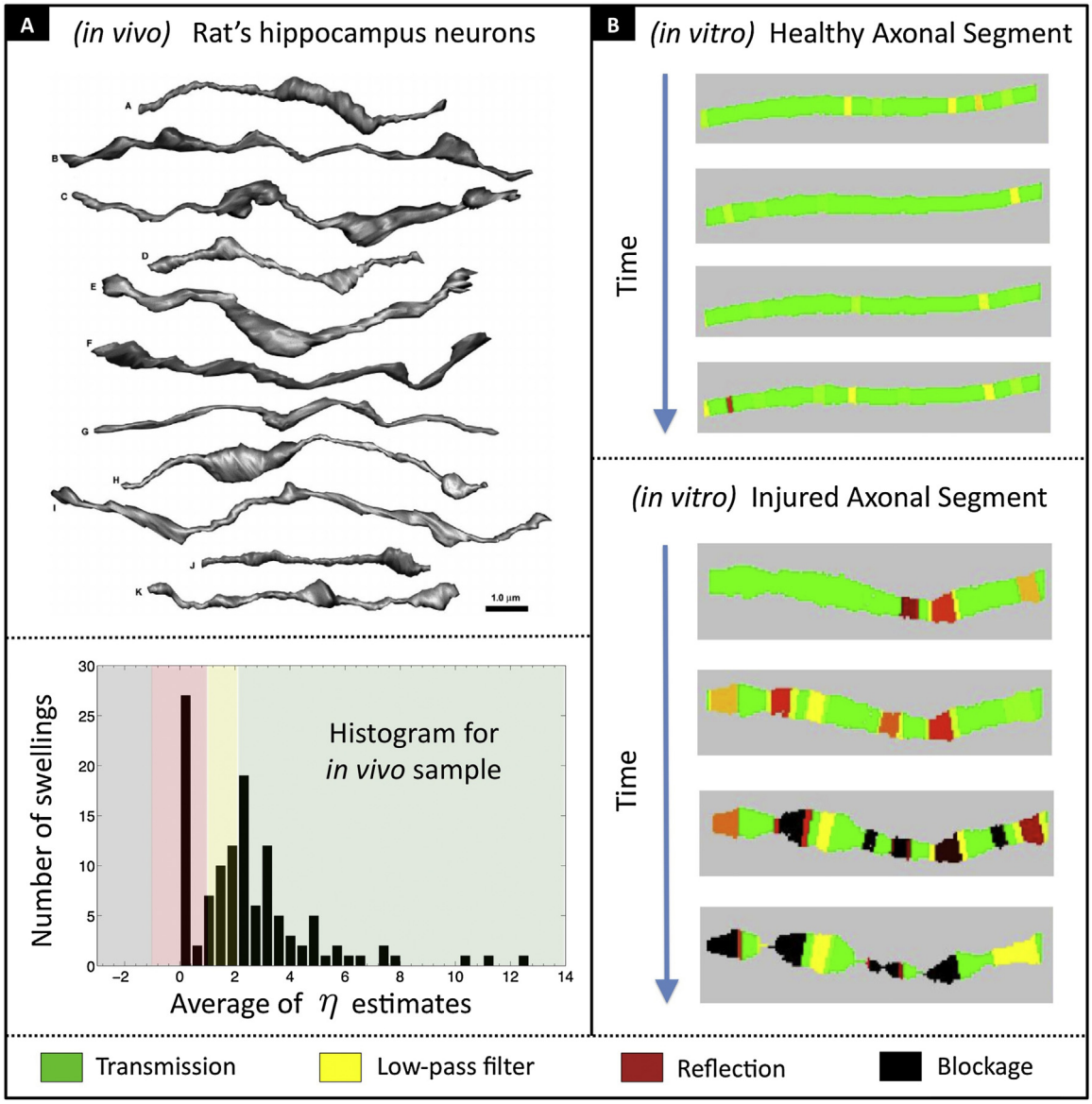

Fig. 2. Panel A: Membrane contours for reconstructed unmylienated axon segments of CA3 → CA1 rat Hippocampal neurons. Courtesy of *SynapseWeb*, Kristen M. Harris, PI, from Shepherd and Harris (1998). Below, we show the corresponding swelling distribution among different functional propagation regimes (transmission, low-pass filter, reflection and blockage). Panel B: Typical evolution of swellings in healthy and injured axonal segment. Axonal coloring diagnostic (axon directionality: left → right) will be detailed in further sections. *In vitro* injury experiments performed by Dr. Matthew Hemphill at Disease Biophysics Group, Wyss Institute for Biologically Inspired Engineering, Harvard University.

the spike train propagation on a number of axons that are calibrated to biophysically realistic geometrical parameters. A full quantification of the axon shaft is also demonstrated, where traffic congestion maps inspire a novel representation of the deleterious effects of FAS. In Section 5 we discuss limitations of our toolbox and important remarks for users. The paper is concluded in Section 6 with an outlook for the developed algorithms and perspectives for future work.

2. Background

2.1. Role of axonal geometry in spike propagation

The classical view on axons as cables that simply transmit spike train encodings is continuously being challenged and revisited as we learn more about their role in signal and information processing (Bucher and Goaillard, 2011; Debanne et al., 2011). Specifically, the interplay between nonlinearities resulting from ion channel properties and geometric inhomogeneities alters the signal before its arrival at synaptic sites. The effects of axonal geometry are even more dramatic in neuronal dysfunctions where effects from axotonomy, regional compaction and Focal Axonal Swellings are implicated (Kolaric et al., 2013). By compromising spike train propagation, axons thus play a critical role in the loss of transmitted information in neuronal networks.

2.2. The spike propagation regime number η

This section reviews how differences in the geometrical tapering parameters of an axonal enlargement can alter spike train propagation properties (Maia and Kutz, 2014a,b). Fig. 3A illustrates a series of spike trains that are reshaped as they travel through an axonal

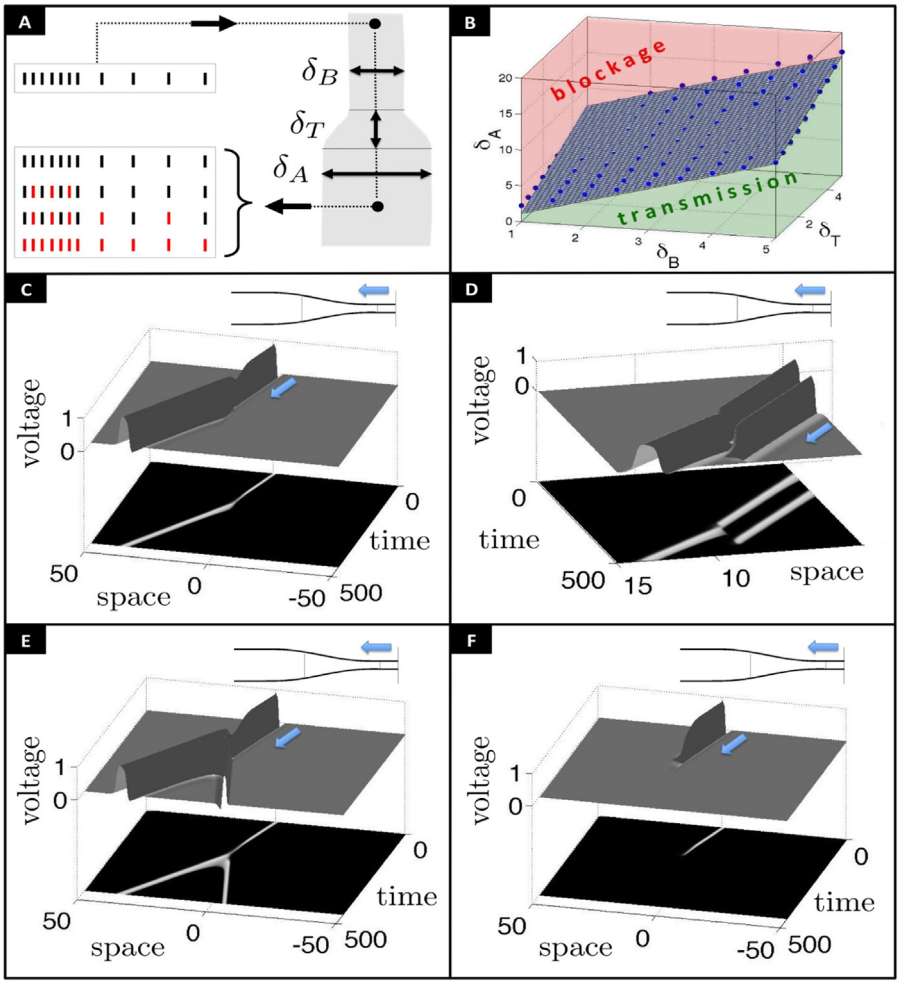

Fig. 3. Axonal geometry defines spike propagation regime. Panel A: Spike trains can be reshaped as they travel along an axonal enlargement. Individual spikes can have their speed changed or even deleted (red). The geometrical tapering parameters $[\delta_B, \delta_T, \delta_A]$ play a key role. Panel B: Explores the parameter space and maps parameter values to their corresponding regime. Panel C: Transmission regime with speed change. Panel D: Filtering regime, where the second spike is deleted and only the first one transmits. Panel E: Reflection regime, where the pulse splits into two, one propagating forward and the other backwards. The backwards propagating pulse will delete the next pulse in the spike train sequence. Panel F: Blockage regime, where no spikes transmit. (For interpretation of the references to color in this figure legend, the reader is referred to the web version of this article.)

Modified from Maia and Kutz (2014b) and Maia and Kutz (2014a).

swelling. Spikes can have their speed changed, reflect or even be deleted (red) depending on the three critical parameters:

δ_B = diameter before

δ_T = diameter of transition

δ_A = diameter after.

By exploring the geometrical parameter space associated with these parameters (Fig. 3B), it is possible to assess individual swellings and their impact on the propagation of an individual spike. Three possibilities exists (Maia and Kutz, 2014a,b): (i) transmission, but potentially with speed changes, (ii) reflection, and (iii) blockage (deletion).

Individual spikes, however, are generically part of a larger cohort of spike trains. Thus from a broader viewpoint, the effects on individual spikes can be translated to an evaluation of spike trains. Indeed, we can map any given axonal enlargement to its functional response on spike train encodings. The following possibilities exist in order of increasing damage: transmission of the spike train with speed changes (Fig. 3C), low-pass filtering of high firing rates due to pile-up collisions and deletions of selected spikes (Fig. 3D) Maia and Kutz (2014a), spike reflections that also lead to a low-pass filtering on both high and low firing rates (Fig. 3E), and spike train blockage (Fig. 3F). The relation between the axonal enlargement parameters and the propagation regimes is well captured by the simple function η (Maia and Kutz, 2014b):

$$\begin{aligned}\eta(\delta_B, \delta_T, \delta_A) &= A + B\delta_B + C\delta_T - \delta_A \\ &= \begin{cases} \gg 1 & \text{for Transmission} \\ \approx 1 & \text{for Filtering} \\ \approx 0 & \text{for Reflection} \\ \ll -1 & \text{for Blockage,} \end{cases} \end{aligned} \quad (1)$$

where $A = -1.842$, $B = 2.284$ and $C = 1.415$. This equation predicts trouble regions in axon geometries and will be used throughout the rest of the work. We remark that the η estimate needs to be calibrated, as detailed in later sections, to specific physiological settings in order to be of quantitative predictive value. It should be noted that many experimental works corroborate this analysis by demonstrating that abrupt or gradual changes in the axonal diameter can delay (Manor et al., 1991; Segev and Schneidman, 1999), block (Goldstein and Rall, 1974; Zhou and Bell, 1994; Altemberger et al., 2001; Kolaric et al., 2013) or reflect a single action potential (Ermentrout, 2010; Rinzel, 1990; Altemberger et al., 2001). Such

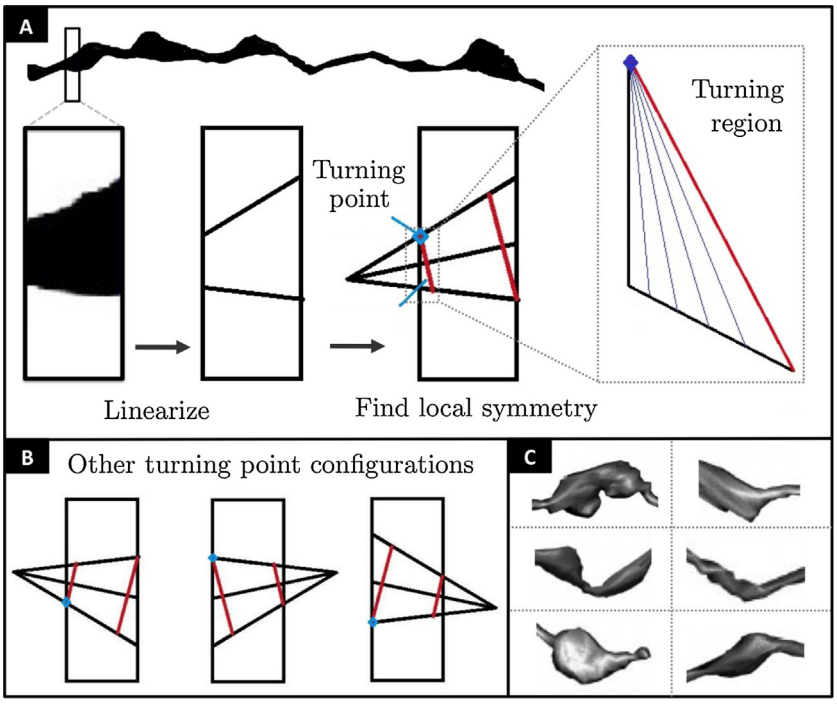

Fig. 4. Extracting axonal cross-section. Panel A: Axonal contours are approximated by patched trapezoids. A non-symmetric trapezoid can be decomposed into a turning region (zoomed) and a symmetric trapezoid (red). One of the vertices is the turning point. Panel B shows other turning point configurations. The algorithm of Section 3.1 handle nontrivial enlargements such as those in Panel C. (For interpretation of the references to color in this figure legend, the reader is referred to the web version of this article.)

biophysical evidence in combination with theoretical studies form the foundations of the present work.

3. Materials and methods

To evaluate the critical parameter η across an axonal segment, the geometrical features of a given axonal swelling must be extracted from a time sequence of axonal images. As a first step, we apply techniques from statistical shape analysis to fix distortions caused by experimental contrast issues in the image acquisition. This technique may be used in combination with more typical image-processing tools (enhance contrast, sharpen edges, adjust colors, crop image, etc.) and must be tailored to the specific set of images being used. In any case, after accounting for the distortions, we then extract the axonal cross-section.

3.1. Extracting axonal cross-section

We now outline our algorithm to extract axonal cross-sections from the captured images (see Fig. 4):

1. Pre-process each image to prune individual axon segments and reduce imaging noise. Convert the image to a grayscale data matrix M_{ij} whose entries vary between zero (black) and one (white). Enhance contrast by applying a threshold τ, i.e., set

$$M_{ij} = \begin{cases} 0 & \text{if } M_{ij} < \tau, \\ 1 & \text{if } M_{ij} > \tau. \end{cases}$$

2. Locate upper and lower axonal contour points by verifying neighboring entries in M where there is a transition from black to white and vice-versa.
3. Approximate the axon segment with patched *trapezoids*, each composed of two vertices in the upper axonal contour and two from the lower axonal contour. The problem is now reduced to extracting the cross-section of each trapezoid.
   - If the trapezoid is symmetric the discrete cross-section values are simply the segments connecting the upper contour vertices to the lower contour vertices.
   - If the trapezoid is non-symmetric, it can be decomposed into a *turning region* patched to a symmetric trapezoid. One of the vertices is the *turning point*. Our cross-section linearly interpolates the turning region until the start of the symmetric trapezoid component. See Fig. 4A for details.

In Fig. 4B we display three prototypical configurations of turning points and turning regions. Thus the method can extract the geometrical features associated with non-trivial axonal sections such as those of Fig. 4C. We remark that there is a simple criteria for determining which vertex is the turning point. As illustrated in Fig. 5A, there are two left angles $[\theta_u, \theta_l]$ associated with a non-symmetric trapezoid. The turning point is always *opposite to the larger angle*. By approximating an axon with a set of turning regions patched to symmetric trapezoids, we can systematically extract its cross-section. The algorithm can be iteratively applied in order to refine the grid as necessary. Fig. 5B applies the algorithm to a typical axon segment and the results are illustrated for this process.

3.2. Image correction via Procrustes superimposition

Time lapse fluorescence imaging of axons in vitro provides the opportunity to visualize changes in axonal morphology. Using this technique, changes in axonal shape have been observed in response to the application of mechanical force (Magdesian et al., 2012; Hemphill et al., 2011). In order to accurately measure relative changes in axonal morphology, it is necessary to account for potential image distortions that may arise due to changes in lighting, cell marker fluorescence levels, or microscope drift. These distortions can lead to incorrect measurements of the geometrical

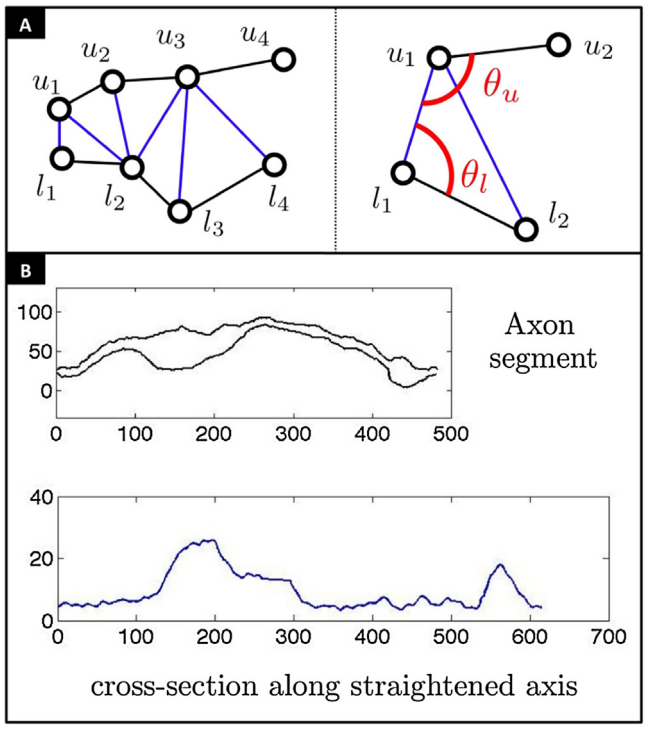

Fig. 5. Criteria to find the turning point. Panel A depicts the left angles $[\theta_u, \theta_l]$ associated to a non-symmetric trapezoid with vertices $\{u_1, u_2, l_1, l_2\}$. The turning point is always the vertex *opposed to the larger angle*. Panel B shows a typical result of the axonal cross-section extraction algorithm of Section 3.1.

parameters of the axon and consequently to a misleading FAS diagnosis (see Fig. 6A). Procrustes analysis can be utilized in order to properly compare the shape of two or more objects in a sequence by optimally translating, rotating, and scaling the objects, prior or after measuring its morphological parameters. Fig. 6B illustrates this methodology pictorially for a few arbitrary shapes. The same principles can also be applied to axon segments.

In statistical shape analysis, a *shape S* is defined as a collection of data points where their cartesian coordinates are stored in a matrix. In the context of an axon, it refers to all the points comprising the axon segment and/or its contour. To optimally superimpose shape S_A to shape S_B we minimize what is called the Procrustes distance between these objects:

$$\begin{aligned} &\text{find} && \text{scaling factor } b > 0, \text{ a rotation matrix } R, \\ &&& \text{and a shift vector } c \\ &\text{to minimize} && ||S_B - b \cdot S_A \cdot R + c||_2, \end{aligned} \tag{2}$$

where the goodness-of-fit criterion is the sum of squared errors. This step may be used to improve a set of images before radius extraction or used to correct the extracted radii afterwards. Fig. 6C exemplifies a contrast issue successfully resolved using the least-square optimization procedure `procrustes.m`. from the MATLAB Statistics and Machine Learning Toolbox.

3.3. Characterizing spike propagation

By using the extracted cross sections of the axonal geometry, such as the one in the bottom panel of Fig. 5, the FAS can be

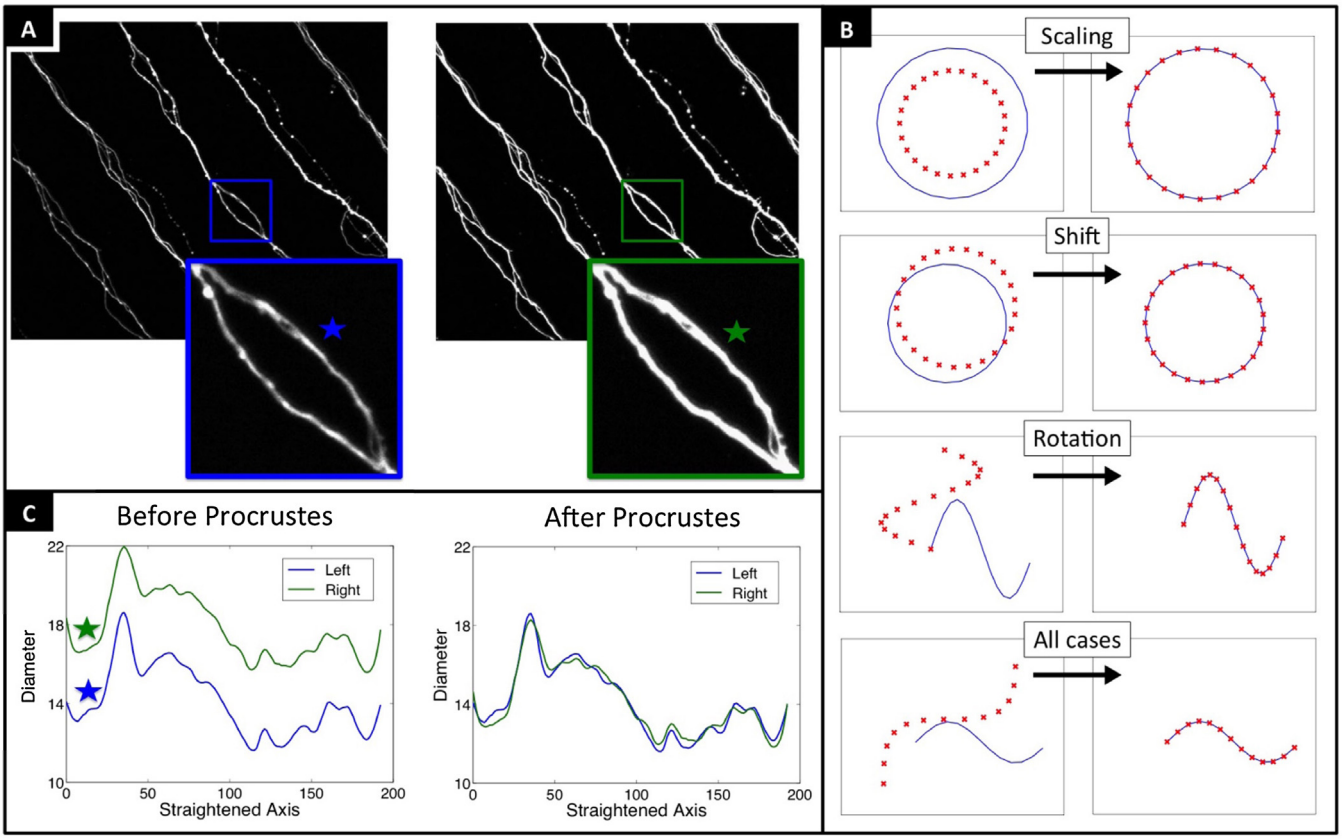

Fig. 6. Shape comparison after Procrustes superimposition. Panel A: Pictures taken with a 5 min interval display contrast problems from experimental artifacts. The right zoomed segment (green) appears larger than the left zoomed segment (blue) even if no significant biological change occurred. Panel B: Procrustes superimposition is an algorithm in statistical shape analysis that can be used to align *arbitrary* shapes via scaling, shifting, rotation and/or a combination of such effects. Panel C: By applying Procrustes superimposition to the highlighted segments, we obtain the optimal factors to correct the contrast issues. See Section 3.2 and the procedure `procrustes.m`. from the MATLAB Statistics and Machine Learning Toolbox for details. (For interpretation of the references to color in this figure legend, the reader is referred to the web version of this article.)

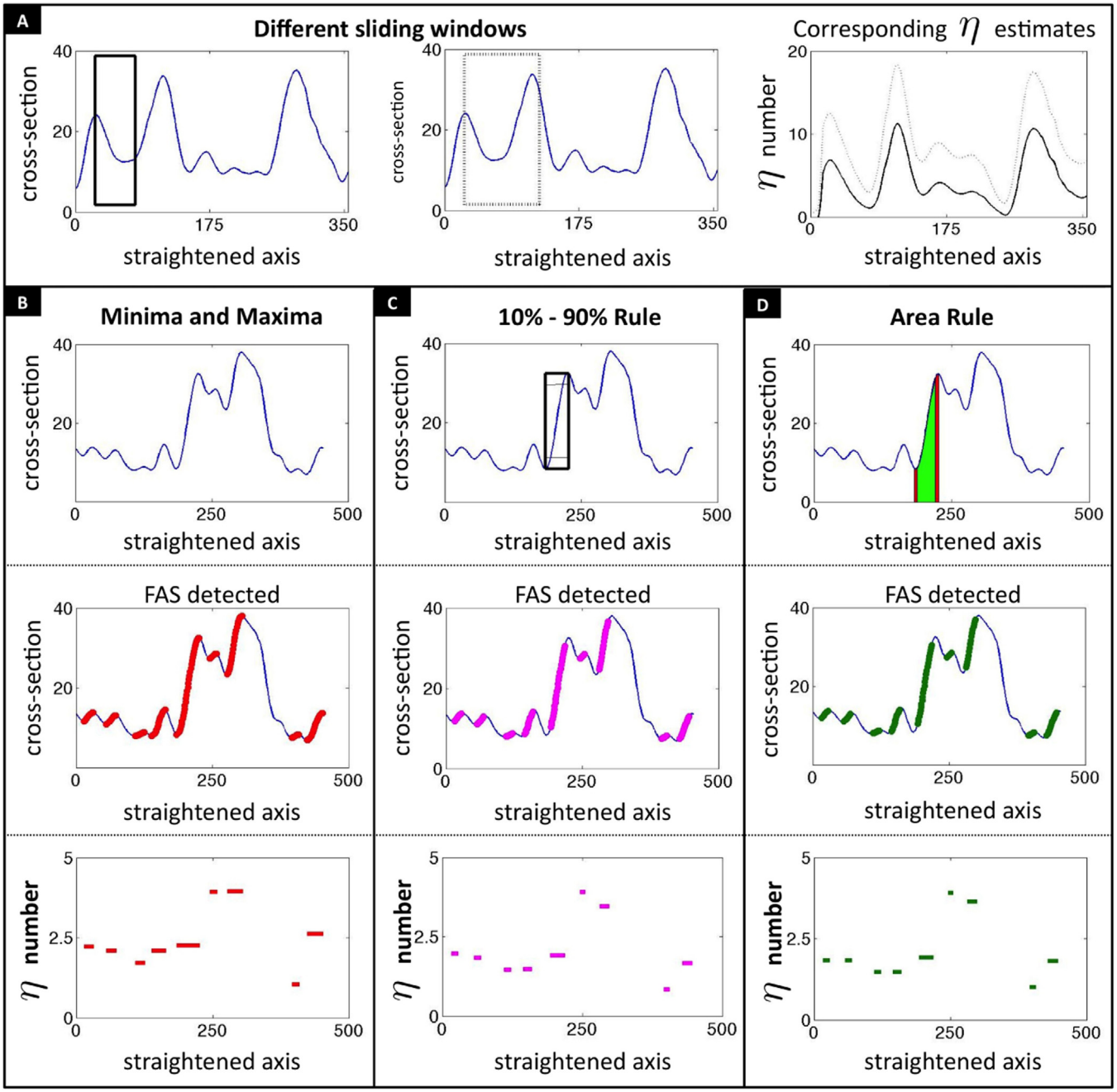

Fig. 7. η estimates from axonal cross-sections (axon directionality: left → right). Panel A illustrates the *sliding window* method with two window sizes and their corresponding η estimates. Panel B illustrates the *minima/maxima* method with the axonal cross-section (top), swelling locations (middle) and the corresponding η estimates (bottom). Panel C illustrates the *10–90% rule* regarding total diameter change and Panel D: the same rule regarding total area change. Panels C and D show the axonal cross-section (top), swelling locations (middle) and the corresponding η estimates (bottom).

characterized along the axon segment. The characterization of the axon segment is done by evaluating the parameter $\eta(\delta_B, \delta_T, \delta_A)$ as a function of distance down the axon. However, the effects of η were associated with the highly idealized geometric structure of Section 1. Real axons have much more challenging geometries then the idealized case, thus requiring further innovations around how to process their structure. The following algorithm is a principled way to deal with the complications of more realistic structures.

Sliding windows. The idea behind this method is to slide parameter-extracting windows of various sizes along the axonal cross-section plots. This technique is reminiscent of a windowed Fourier transform where time-frequency localization can be computed with a spectrogram. Here, the sliding window is used instead to capture FAS events and the geometrical associated with them. See Fig. 7A for an example. As the window slides, it follows some rules to extract $[\delta_B, \delta_T, \delta_A]$ from the portions of the axonal diameter $d(x)$ contained in it. Specifically:

1. Set the length L of the parameter-extracting window and let $d_{\max} = d(x_{\max})$ be the maximal diameter value contained in $[x, x+L]$.
2. If $x_{\max}$ is the first point in the window, set

$$\delta_B = d_{\max}, \quad \delta_T = L, \quad \text{and,} \quad \delta_A = d(x+L),$$

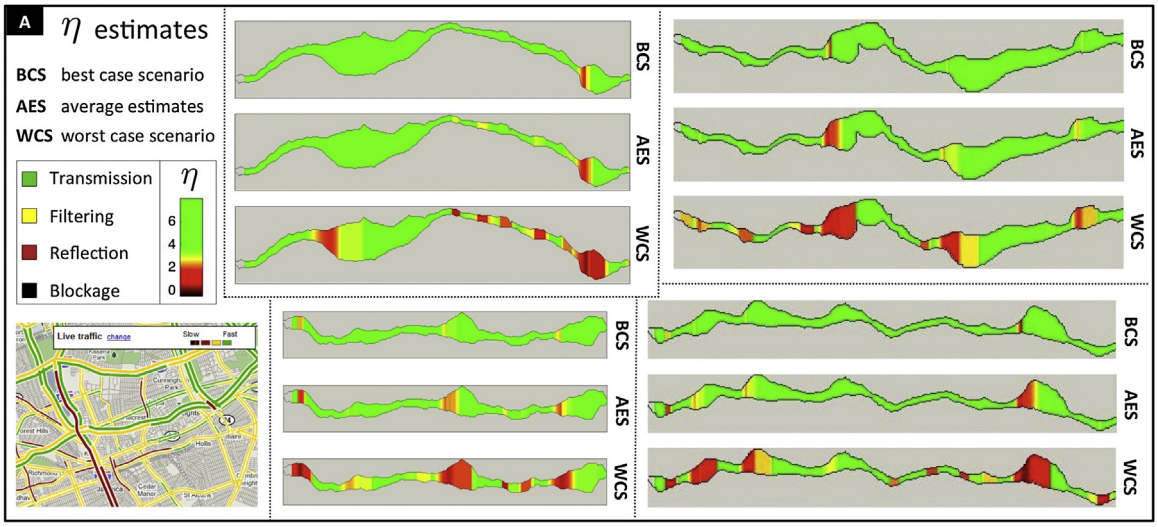

Fig. 8. Four axon segments modified from *SynapseWeb*, Kristen M. Harris, PI, from Shepherd and Harris (1998). Each axon segment is color-coded spatially according to the propagation regime number η (axon directionality: left → right). Different criteria lead to different η estimates, and there are multiple ways to integrate them: best case scenario (BCS), average estimates (AES) and worst case scenario (WCS). These plots are analogous to car traffic maps (bottom left) that can identify blocked or impaired routes for signal flow. This framework could lead to important improvements in FAS (cognitive deficit) diagnostics and to our understanding of the several pathologies in which they are implicated.

otherwise, set

$$\delta_B = d(x), \quad \delta_T = x_{\max} - x, \quad \text{and,} \quad \delta_A = d_{\max}.$$

As we slide the parameter-extracting window, η is continuously calculated along the axon segment. Estimates of η vary considerably with the window lengths (see Fig. 7A); larger windows can contain multiple FAS whereas smaller windows may not capture an entire swelling due to the limited window size. The method may also handle swollen and non-swollen regions of the axon indistinguishably.

Minima and maxima. To refine the estimates above, we recalculate η for each FAS. They are located by properly pairing the extrema of the diameter function, with each swelling starting at a local minimum $x_{\min}$ and ending at the next local maximum $x_{\max}$. Then, we assign for each located swelling:

$$\delta_B = d(x_{\min}), \quad \delta_T = x_{\max} - x_{\min}, \quad \text{and,} \quad \delta_A = d(x_{\max}).$$

Constant values of η for each swelling provide clearer diagnostic interpretations (see Fig. 7B). This method works well for swellings with linear diameter growth but might fail for those with sigmoid shapes. If the detected swellings include large flat sections of the axonal diameter, δ_T can grow disproportionately to δ_A and δ_B. Since flat regions are not expected to interfere significantly with the propagating signal (Maia and Kutz, 2014b), it helps to trim them off from the detected swellings.

The 10–90% rule. To revise the swelling's endpoints, we borrow an idea from electronic signal processing (Marcuse, 1974): we set the left and right limits where the total diameter increase – or total area increase – reaches 10% and 90% respectively, hence the name of the rule. The η estimates are now calculated from the revised endpoints (see Fig. 7C and D). The two variants of the rule agree in the majority of cases and return values of η typically smaller than the other methods.

Combining estimates. These algorithms produce a set of η estimates which we combine in different ways: (1) best-case scenario, (2) worst-case scenario and (3) average estimates. In the best/worse case scenario we overwrite sliding window estimates with those taken from the extrema and/or 10–90% rules. In the third case, we average all estimates along the axonal axis. These various estimates for η are pursued in order to provide a more robust measure of the effects associated with FAS.

4. Results

Our combined algorithms color-code swellings along axonal segments as displayed in Fig. 8; we show four axonal segments from the set of *SynapseWeb*, Kristen M. Harris, PI, from Shepherd and Harris (1998). The plots are analogous to traffic maps that depict congested areas of traffic by color coding. Specifically this traffic map can identify – for spike train encodings and signal flow – blocked or impaired routes. One should simply keep track of where the color changes from green to yellow (filtering of spikes), to red (spike reflection), or to black (spike blockage), in order to identify regions where transmitted information is lost.

We used three different criteria to combine the multiple η estimates: best case scenario (BCS), average estimates (AES) and worst case scenario (WCS). They can differ significantly in the assessment of the propagation regimes; However, having multiple ways to combine η estimates allow more flexibility to calibrate our geometrical measurements to the specific physiological settings of the analyzed neuron. In Fig. 8, for example, we normalized the geometrical parameters such that the smallest cross-section value of our sample to matches the smallest radius of the simulations in Maia and Kutz (2014b). This matching step is not universal (since the η-parameters are given in non-dimensional units) and may vary depending on the properties of the axons involved. Hence, when we display a critical enlargement, it is relative only to neurons of the same organism and type. The rationale is that the user will *calibrate* the toolbox to his/her own dataset, trying to:

1. Study the natural changes in the geometry of healthy axons and the statistics of their geometrical parameters.
2. Enforce $\eta \gg 1$, i.e., spike propagation in transmission regime for these axons.
3. Find $\eta < 1$ for large and/or abrupt axonal swellings for injured axons. This is a good indication that trouble in spike propagation might occur in that swelling.

The theoretical predictions of blockage, reflection, or filtering of spikes may not match since there are many other factors that influence neuronal electrophysiology (see Section 5). The main advantage of the method is the ability to compare swellings of various shapes *relative* to each other. We believe this framework is a promising starting point for diagnosing axonal swellings implicated in several neuropathologies.

5. Discussion

In this section we make important remarks for users and discuss limitations of the underlying theoretical framework and of the computational toolbox.

5.1. Calibrating estimates to specific datasets

The calibration process demonstrated above is critical in diagnosing neuronal injury. Specifically, geometrical parameters for axons can vary significantly between species (e.g., human versus rodent versus the giant squid axon). Additionally, within a given species neurons can be substantially different depending upon their functionality and/or region in which they are active (e.g., hippocampal versus cortical neurons). Finally, the composition of the cytoskeleton determines many of the elastic properties of a neuron, making some neurons potentially more prone to FAS injury than others. Thus in the calibration process, it is imperative to evaluate neurons drawn independently from the same class and/or functional areas. Interestingly, the variety of neurons present in a single species suggests a comparative study aimed at evaluating the robustness of different neuron types to injury. This will be explored further in future work.

6. Limitations of theoretical estimates

The η-regime framework was pointed out to have several limitations. In fact, Maia and Kutz (2014b) wrote explicitly in their original paper: "The biophysics of our AP model is over-simplified (...), but it can be improved by adding synapses, non-uniform distributions of ion channels and a more complete set of ionic currents. We assumed, for example, that the varicosities were made of the same material as the axoplasm. It is likely that a constant resistivity value along the entire axon might not hold. Additionally, most axonal varicosities contained mitochondria (that regulate presynaptic Ca^{2+}) or other possibly electrically active vesicles that were not taken into account by our model. Better quantification of their electrophysiological properties and others, such as distributions of ion channels, pumps, buffers and other molecules, will be required for ideal biophysical modeling." Still, anomalous changes in geometry are an important proxy to harmful Focal Axonal Swellings.

The estimation method presented is also limited to *local* propagation properties of Action Potential (AP), i.e., anomalous effects are constrained to the vicinity of each FAS. However, some of these effects might affect signal transmission along the entire neuron. For example, when there is AP reflection due to FAS the entire proximal axonal segment would no longer allow normal transmission due to collision of orthodromic and antidromic APs. In fact, reflected APs have been observed in a variety of neuronal systems (Baccus, 1998; Baccus et al., 2000; Debanne et al., 2011; Goldstein and Rall, 1974; Parnas, 1979; Ramon et al., 1975). This makes diagnosing injured axons even harder, since the source/cause of spatiotemporal anomalies might be relatively far from where they are observed in the axon.

6.1. Limitations of the computational toolbox

It is hard to anticipate the properties of multiple types of axonal images produced by different experimental setups regarding colors, scales, resolution, etc. Our toolbox is in its infancy and consequently can only handle a few formats in an automated way. In extracting the axonal contour, the cut-off frequency of the low pass filter may need adjustments depending on the image resolution. Too much smoothing would affect the η value since the abrupt change of the diameter is critical for the axonal conduction. Also, if noisy pixels exist outside the axon, it may overestimate the axonal diameters. Finally, the precision and limits of the computational toolbox may vary. There will be a chance that normal varicosities may be interpreted as pathological swellings and vice versa, since the η criterion is purely geometrical. The toolbox will work better when swellings arising from traumatic axonal injury are significantly different than natural varicosities. Results are likely to improve if the user tracks the geometry of the same axon before and after injury to discount for natural varicosities.

Despite all limitations described above, we would argue that changes in morphology do give important clues of trouble spots for spike propagations. The η estimates are – with all their flaws – the best currently available theoretical relations between axonal geometry and spike propagation (Maia and Kutz, 2014b,a). The careful extraction of geometrical parameters from complex morphologies is not straightforward and required specialized algorithms in some harder cases. Finally, we expect to develop better methodologies, protocols and standards to improve these issues in future works, taking into account our future user's feedback and requests.

7. Conclusion

Focal Axonal Swellings (FAS) are ubiquitous to some of the most prominent neuro-degenerative diseases of the central nervous system such as Alzheimer's and Parkinson's diseases, Multiple Sclerosis and others (Millecamps and Julien, 2013; Coleman, 2005; Tsai et al., 2004; Krstic and Knuesel, 2012; Galvin et al., 1999; Liberski and Budka, 1999; Adle-Biassette et al., 1999; Ferguson et al., 1997; Trapp et al., 1998). FAS are also hallmark features of concussions and traumatic brain injuries (Fainaru-Wada and Fainaru, 2013; Jorge et al., 2012; Xiong et al., 2013).

This work reinforces recent findings that the shape of the FAS are essential for assessing the post-injury capabilities of axons (Maia and Kutz, 2014a,b; Kolaric et al., 2013; Altemberger et al., 2001). TBI studies demonstrate that FAS can induce up to a 30-fold increase in axon diameter (Tang-Schomer et al., 2012, 2010). Here we combined geometrical tapering parameters with theoretical estimates to provide valuable insight on critical regions for spike propagation; Large swellings with a smooth cross-sectional increase might not significantly alter electrophysiological signaling whereas smaller FAS with abrupt diameter changes are especially prone to blockage or loss of transmitted information.

It is important to recognize the role of FAS geometry for the broader research community especially when there are no well-established protocols to measure geometrical properties of FAS (Magdesian et al., 2012; Hemphill et al., 2011; Smith et al., 1999; Maxwell et al., 1997). In fact, it can be challenging to characterize FAS geometry in a principled, general, and adaptive way. Thus, we developed novel algorithms and/or tailored existing ones to address the need to better classify, quantify, and diagnose FAS. We used procrustes superimposition to fix image artifacts and extracted axonal cross-section with patched trapezoids alternated with turning regions. From these cross-section results, we used different rules (sliding windows, maxima and minima, 10–90% rule) to estimate the tapering parameters $[\delta_B, \delta_T, \delta_A]$ (see Fig. 3A)

necessary to calculate the η estimates and the corresponding spike propagation regime (see Eq. (1)).

Some of the limitations of our work include the fact that the η estimates were derived for unmylienated FitzHugh-Nagumo neuron models (Maia and Kutz, 2014a,b). This model might not be suited for all physiological settings and may require specific calibrations and/or other adjustments. Regardless, if new η estimates become available for different neuronal settings, they can be easily incorporated into the MATLAB toolbox developed for this work.

Overall, one of the challenging aspects of research in neurodegenerative diseases and TBI is understanding how neuronal pathologies developed at a cellular level (Johnson et al., 2013; Morrison et al., 2011) compromise the functionality of an entire network of neurons. Many studies reported cognitive, behavioral, perceptual and sensory-motor impairments resulting from such disorders, yet no framework could link these macro scale symptoms to the FAS pathologies observed at the cellular level, or micro scale (Magdesian et al., 2012; Hemphill et al., 2011; Smith et al., 1999; Maxwell et al., 1997). Our toolbox provides – in analogy to car traffic maps – a way to identify blocked or impaired routes for spike train encodings and signal flow. By keeping track of where axonal color-code changes from green to yellow (filtering of spikes), to red (spike reflection), or to black (spike blockage), an evaluation of potential cognitive impairment can be made. We believe this framework is a promising starting point for diagnosing axonal swellings and consequently the neurodegeneratve disorders in which they are implicated.

Appendix A. MATLAB Toolbox

Our toolbox is compatible with MATLAB's R2014b and R2012b versions, and require functions from the *Curve Fitting Toolbox*. The basic outline of the code is to

1. Select an axon image with `imread` command.
2. Extract the axonal membrane contours with `core_axon_radius.m`.
3. Create a structure to store η estimates and other important geometrical parameters with `core_axon_structure.m`.
4. Plot and display these estimates with `core_axon_structure_plots.m`.
5. Color-code the axon with a customized colormap using the `core_painter.m` function.

Axon images must depict a single horizontally displayed axonal structure (in white) tightly cropped against a black background, preferentially in JPEG format. The axon directionality is assumed to be from left to right. For examples see the pre-processed set of membrane contours {`KH01.jpg`, `KH02.jpg`, . . ., `KH11.jpg`} that depicts reconstructed unmylienated axon segments of CA3 → CA1 rat Hippocampal neuron – courtesy of *SynapseWeb*, Kristen M. Harris, PI, from Shepherd and Harris (1998).

Run `demo1.m` to see the original `KH08.jpg` axonal image, the corresponding cross-section along it's straightened axis (like in Fig. 5B) and several η estimates (like in Fig. 7). It is straightforward to select another axon from the set by changing the name in the `imread` line in the `core_painter.m` file. We suggest users to modify `demo1.m` when trying to use their own datasets.

Run `demo2.m` to color-code all 11 axons from the dataset with all three different criteria to combine the multiple η estimates: best case scenario (BCS), average estimates (AES) and worst case scenario (WCS). The `core_painter.m` function might not match the increases in radius exactly and distortions are higher when the axon is bended, twisted or asymmetric. Thus, the color-coded axons should be regarded as a proxy for the more precise `core_axon_structure_plots.m`. See the companion pdf file for details.

References

Adle-Biassette H, Chretien F, Wingertsmann L, Hery C, Ereau T, Scaravilli F, Tardieu M, Gray F. Neuronal apoptosis does not correlate with dementia in HIV infection but is related to microglial activation and axonal damage. Neuropathol Appl Neurobiol 1999];25:123–33.

Altemberger R, Lindsay K, Ogden J, Rosenberg J. The interaction between membrane kinetics and membrane geometry in the transmission of action potentials in non-uniform excitable fibres: a finite element approach. J Neurosci Methods 2001];112:101–17.

Baccus S. Synaptic facilitation by reflected action potentials: enhancement of transmission when nerve impulses reverse direction at axon branch points. Proc Natl Acad Sci 1998];95(14):8345–50.

Baccus S, Burrell B, Sahley C, Muller K. Action potential reflection and failure at axon branch points cause stepwise changes in EPSPs in a neuron essential for learning. J Neurophysiol 2000];83(3):1693–700.

Bucher D, Goaillard JM. Beyond faithful conduction: short term dynamics, neuromodulation, and log-term regulation of spike propagation in the axon. Prog Neurobiol 2011];94:307–46.

Coleman M. Axon degeneration mechanisms: commonality amid diversity. Nat Rev Neurosci 2005];6(11):889–98.

Debanne D, Campanac E, Bialowas A, Carlier E, Alcaraz G. Axon physiology. Physiol Rev 2011];91:555–602.

Ermentrout G. Mathematical foundations of neuroscience. Springer; 2010].

Fainaru-Wada M, Fainaru S. League of denial: the NFL, concussions, and the battle for truth. Crown Archetype 2013].

Ferguson B, Matyszak MK, Esiri MM, Perry VH. Axonal damage in acute multiple sclerosis lesions. Brain 1997];120:393–9.

Galvin JE, Uryu K, Lee VM, Trojanowski JQ. Axon pathology in Parkinson's disease and lewy body dementia hippocampus contains α-, β-, and γ -synuclein. Proc Natl Acad Sci 1999];96:13450–5.

Goldstein S, Rall W. Changes of action potential shape and velocity for changing core conductor geometry. Biophys J 1974];14:731–57.

Hemphill M, Dabiri B, Gabriele S, Kerscher L, Franck C, Goss J, Alford P, Parker K. A possible role for integrin signaling in diffuse axonal injury. PLoS ONE 2011];6(7):e22899.

Hemphill M, Dauth S, Yu CJ, Dabiri B, Parker K. Traumatic brain injury and the neuronal microenvironment: a potential role for neuropathological mechanotransduction. Neuron 2015];86(6):1177–92.

Johnson VE, Stewart W, Smith DH. Axonal pathology in traumatic brain injury. Exp Neurol 2013];246:35–43.

Jorge RE, Acion L, White T, Tordesillas-Gutierrez D, Pierson R, Crespo-Facorro B, Magnotta V. White matter abnormalities in veterans with mild traumatic brain injury. Am J Psychiatry 2012];169(12):1284–91.

Kolaric KV, Thomson G, Edgar JM, Brown AM. Focal axonal swellings and associated ultrastructural changes attenuate conduction velocity in central nervous system axons: a computer modeling study. Physiol Rep 2013];1(3):e00059.

Krstic D, Knuesel I. Deciphering the mechanism underlying late-onset Alzheimer disease. Nat Rev Neurosci 2012];9(1):25–34.

Liberski PP, Budka H. Neuroaxonal pathology in Creutzfeldt-Jakob disease. Acta Neuropathol 1999];97:329–34.

Magdesian MH, Sanchez FS, Lopez M, Thostrup P, Durisic N, Belkaid W, Liazoghli D, Grütter P, Colman R. Atomic force microscopy reveals important differences in axonal resistance to injury. Biophys J 2012];103(3):405–14.

Maia PD, Kutz JN. Compromised axonal functionality after neurodegeneration, concussion and/or traumatic brain injury. J Comput Neurosci 2014a];27:317–32.

Maia PD, Kutz JN. Identifying critical regions for spike propagation in axon segments. J Comput Neurosci 2014b];36(2):141–55.

Manor Y, Koch C, Segev I. Effect of geometrical irregularities on propagation delay in axonal trees. Biophys J 1991];60:1424–37.

Marcuse D. Theory of dielectric optical waveguides. Academic Press; 1974].

Maxwell WL, Povlishock JT, Graham DL. A mechanistic analysis of nondisruptive axonal injury: a review. J Neurotrauma 1997];17(7):419–40.

Millecamps S, Julien J. Axonal transport deficits and neurodegenerative diseases. Nat Rev Neurosci 2013];14(161):161–76.

Morrison B, Elkin BS, Dolle JP, Yarmush ML. In vitro models of traumatic brain injury. Ann Rev Biomed Eng 2011];13(1):91–126.

Parnas I. Propagation in nonuniform neurites: form and function in axons. The Neurosciences. Cambridge: MIT Press; 1979]. p. 499–512.

Ramon F, Joyner R, Moore J. Propagation of action potentials in inhomogeneous axon regions. Fed Proc 1975];34:1357–63.

Rinzel J. Mechanisms for nonuniform propagation along excitable cables. Ann N Y Acad Sci 1990];591.

Segev I, Schneidman E. Axons as computing devices: basic insights gained from models. J Physiol 1999];93:263–70.

Shepherd G, Harris K. Three-dimensional structure and composition of ca3 to ca1 axons in rat hippocampal slices: implications for presynaptic connectivity and compartmentalization. J Neurosci 1998];18(20):8300–10.

Smith D, Wolf J, Lusardi T, Lee V, Meaney D. High tolerance and delayed elastic response of cultured axons to dynamic stretch injury. J Neurosci 1999];19(11):4263–9.

Tang-Schomer MD, Johnson VE, Baas PW, Stewart W, Smith DH. Partial interruption of axonal transport due to microtubule breakage accounts for the formation of periodic varicosities after traumatic axonal injury. Exp Neurol 2012];233:364–72.

Tang-Schomer MD, Patel A, Bass PW, Smith DH. Mechanical breaking of microtubules in axons during dynamic stretch injury underlies delayed elasticity, microtubule disassembly, and axon degeneration. FASEB J 2010];24(5):1401–10.

Trapp B, Peterson J, Ransohoff R, Rudick R, Mrk SBL. Axonal transection in the lesions of multiple sclerosis. N Engl J Med 1998];338:278–85.

Tsai J, Grutzendler J, Duff K, Gan WB. Fibrillar amyloid deposition leads to local synaptic abnormalities and breakage of neuronal branches. Nat Neurosci 2004];7:1181–3.

Xiong Y, Mahmood A, Chopp M. Animal models of traumatic brain injury. Nat Rev Neurosci 2013];14(22):128–42.

Zhou Y, Bell J. Study of propagation along nonuniform excitable fibers. Math Biosci 1994];119(2):169–203.